QM−MM Study of Nitrite Reduction by Nitrite Reductase of *Pseudomonas aeruginosa*

Marcelo A. Martí, Alejandro Crespo, Sara E. Bari, Fabio A. Doctorovich, and Darío A. Estrin*

Departamento de Química Inorgánica, Analítica y Química Física/INQUIMAE-CONICET, Facultad de Ciencias Exactas y Naturales, Universidad de Buenos Aires, Ciudad Universitaria, Pabellón II, Buenos Aires (C1428EHA), Argentina

Received: March 17, 2004; In Final Form: August 18, 2004

The one electron reduction of nitrite to NO, catalyzed in vivo by a group of enzymes called nitrite reductases (NIRs), has been extensively investigated due to its relevance in the processes of denitrification. The heme containing NIRs are soluble noncovalent homodimers with two heme groups in each subunit: a d_1 heme, the site of nitrite reduction, and a type *c* heme, responsible for internal electron transfer. High resolution X-ray structures show that all NIRs have two distal histidines in the active site as a common feature. We analyzed the reaction mechanism of nitrite reduction by *Pseudomonas aeruginosa* (Pa) NIR using a combined quantum mechanics/molecular mechanics (QM−MM) approach. The central Fe(II) porphyrin complex plus the proximal and distal histidines were treated at the density functional theory level, while the solvated protein environment was modeled using the Amber force field. Our results indicate that nitrite binds to the reduced active site with one histidine protonated and that, after protonation of the second histidine, proton transfer and dehydration result in an $Fe^{III}(NO)$ species plus a free water molecule coordinated to both histidines. The computed results also suggest that the NO ligand is probably displaced by another water molecule in the distal cavity. The enzyme finally recovers the resting state, after proton reorganization, reduction, and water formation. Our results show that the catalytic capacity of the enzyme lies primarily on the distal histidines, real guards of the active site cavity.

Introduction

The dissimilatory denitrification pathway represents one of the main branches of the bacterial nitrogen cycle, the set of key processes for nitrogen balance and cellular bioenergetics.[1] Nitrite reductases (NIRs) are a group of enzymes that catalyze in vivo the first step of the nitrogen cycle, yielding a gaseous product: the one electron reduction of nitrite into nitric oxide.[2,3] NIRs have also been found to catalyze in vitro the four electron reduction of dioxygen to water, similarly to membrane bound oxidases.[4] There are two different kinds of NIRs with distinct structures and catalytic sites: the multiheme NIRs and the copper containing NIRs. To date, there is no differential denitrification potential or capability established for each group of NIRs, and they have never been found to coexist in the same bacteria.

The proposed reaction mechanism of multiheme NIRs involves the following steps (Figures 1 and 2): nitrite coordination to the reduced d_1 heme, the formation of an $Fe^{II}(NO^+)$ or an $Fe^{III}(NO)$ species[5] (denoted {FeNO}[6] in the Enemark and Feltham notation),[6] with concomitant dehydration, subsequent release of NO, and an intramolecular electron transfer from the c heme to the d_1 heme to regenerate the active site. The role of NO in denitrification has recently been reviewed by Wasser et al.[7]

Bifunctional, multiheme-containing NIRs are soluble enzymes located in the periplasmic space of bacteria. They have been isolated and purified from a wide variety of bacteria including *Pseudomonas aeruginosa*,[8] *Paracoccus pantotrophus* (formerly *Tiosphaera pantotropha)*,[9−10] *Paracoccus denitrificans*,[11] and *Pseudomonas stutzeri*.[12] The enzymes are noncovalent homodimers with one d_1 heme as the catalytic site and up to five *c* heme groups for electron transport *per* subunit. The high resolution X-ray structures show that each type of heme is located in distinct domains: an N-terminal helical domain contains the *c* heme moieties, and a C-terminal eight-blade β propeller contains the d_1 heme.[7,13,14] The *c* heme acts as an electron acceptor from cytochrome *c*551 or azurin. The d_1 heme is the site of nitrite reduction and is a unique prosthetic group in that the Fe^{III}/Fe^{II} reduction potentials of d_1 heme models are 200 mV less negative than the corresponding ones for isolated iron porphyrins.[15]

Common features in all reported X-ray structures of NIRs are the presence of two invariant histidines and a tyrosine residue in the d_1 heme distal cavity. (His 345, His 388, and Tyr 25 in *Paracoccus pantotrophus* and His 327, His 369, and Tyr 10 in *Pseudomonas aeruginosa*).

The role of the distal histidines has been assessed with two site directed mutants (H369A and H327A). Both histidines have been found to be relevant for nitrite reductase activity, showing only 1% of NIR Pa wild type activity, although no effect was measured for the in vitro dioxygen reduction.[16] The same authors demonstrated with stopped flow experiments that His 369 controls and enhances the affinity for nitrite ligand. Although anion affinities are expected to be lower for the reduced form of the heme enzymes, compared to the oxidized form, the positive charged protonated residues are capable of enhancing them significantly. Another set of mutational experiments was performed to investigate the role of Tyr 10, replacing it for Phe. No differences were found in the nitrite reductase or oxidase activities for this mutant, indicating that Tyr 10 does not play a key role in catalysis.

Cutruzzola et al.[16] suggested that the activity for dioxygen reduction remained unchanged due to the neutral condition of

* To whom correspondence should be addressed. E-mail: dario@qi.fcen.uba.ar. Fax:(5411) 4576 3341.

10.1021/jp048807r CCC: $27.50
Published on Web 10/20/2004

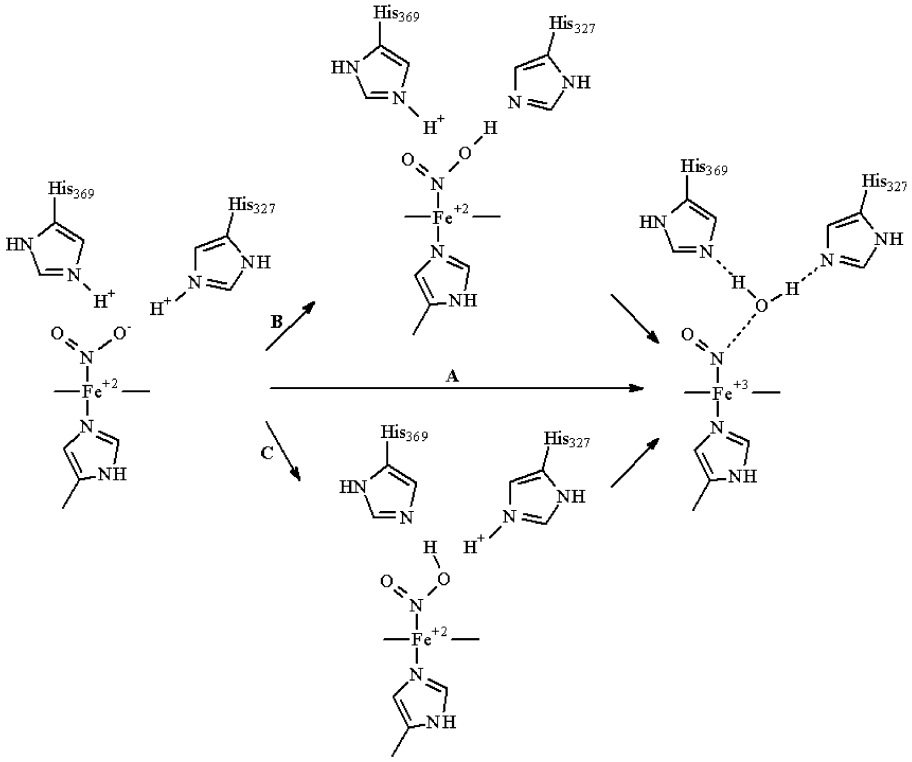

Figure 1. Possible routes for nitrite reduction. The concerted mechanism proceeds directly through path A. The two step mechanism goes through path B or C with their proposed intermediates.

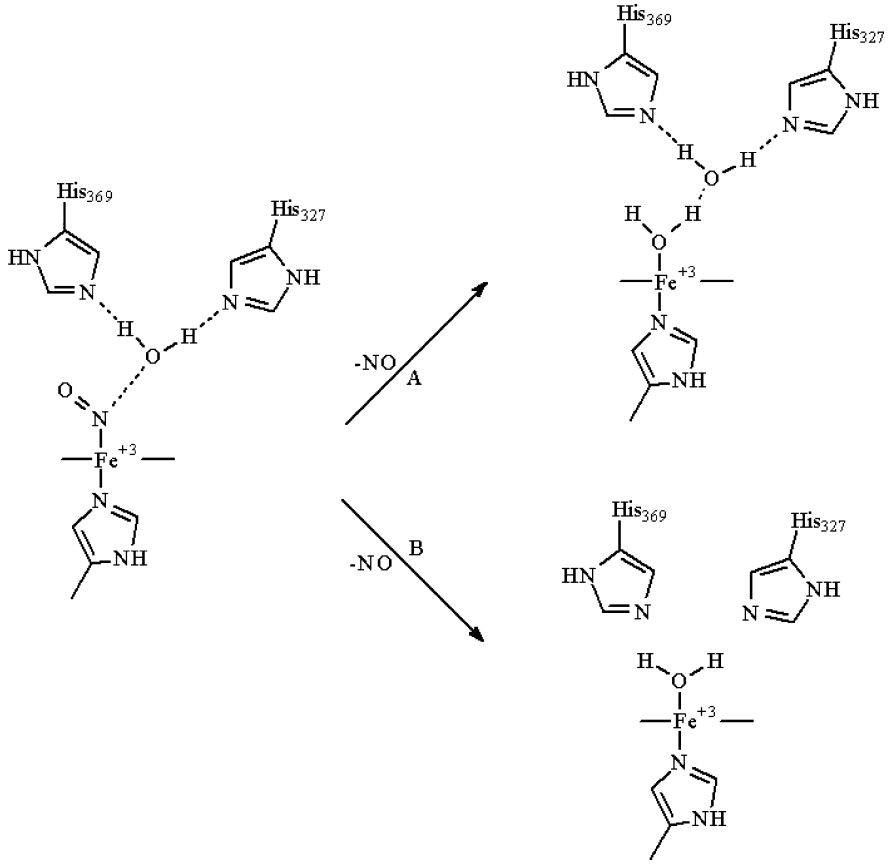

Figure 2. NO release mechanism.

the substrate, which did not require both histidine residues for stabilization, and that the extra proton can be supplied from bulk water, accessible to the distal pocket in the mutated protein.

NO displacement is the key step for the enzyme turnover. In X-ray structures of *Paracoccus pantotrophus*, it has been observed that the distal side of the d_1 heme is occupied by the

oxo group of Tyr 25, which is capable of displacing the NO ligand.[17] However, the lack of homologous N-terminal loops in other species led to the proposal that this oxidized structure represented a nonfunctional resting state.[18,19] In *Pseudomonas aeruginosa*, Tyr 10 residue (homologous to Tyr 25 in *Paracoccus denitrificans)* is not directly bonded to the heme, but it is hydrogen bonded to an hydroxide ion, the sixth ligand of the d_1 heme.[13] In this case, this hydroxide ion has been proposed to induce NO displacement.

A process of internal electron transfer between the His/Met coordinated *c* heme and the hydroxide/His coordinated d_1 heme in the oxidized state has been proposed to explain the reduction of the d_1 heme to the ferrous resting state, where it is only coordinated to His. The *c* heme coordination remains unchanged upon metal reduction.[14]

Quantum mechanical calculations, and particularly those based on density functional theory (DFT) methods, have been demonstrated to be successful in many biochemical applications, specifically in the study of iron porphyrinates and heme containing enzymes.[20−30] A previous theoretical study by Ranghino et al.[31] (using DFT at the local density aproximation) using a stripped down model system of the active site of NIR from *Paracoccus pantotrophus* (Pp) showed the feasibility of a concerted reaction path for the dehydration process in which one of the nitrite oxygen atoms binds to both protons of the protonated distal histidines in one step, leading to the {FeNO}^{6} species. This study also suggested that the NO releasing step in this species could be assisted by a tyrosine and favored by unprotonated histidines. These results provided relevant information about the nitrite reduction mechanism in Pp NIR. However, the inclusion of the whole protein is necessary to obtain a more realistic modeling of the NIR reaction mechanism and to understand the key structural determinants for catalysis.

QM−MM is the method of choice to account for the effect of protein and solvent environments in the detailed study of chemical reactions by computer simulations. The idea of QM−MM was originally introduced by Warshel and Levitt[32] as an efficient way of incorporating the effects of the protein environment on the electronic structure of enzyme active sites. There are several QM−MM schemes available, differing mainly in the electronic structure level treatment of the QM subsystem and the force field implemented.[33−37]

In this work, we provide a complete, detailed microscopic picture of the NIR reaction in Pa obtained by performing QM−MM calculations. The main issues we address are the role of histidine protonation and of the iron oxidation state in nitrite binding, the dehydration mechanism and the associated energy profiles, the mechanism of NO release, the mechanism of avoidance of the {FeNO}^{7} dead end product, and the recovery of the resting state. NIR Pa was chosen by the fact that the overall protein structure, and particularly the vicinity of the active site, does not change significantly along the reaction path as evidenced from the analysis of the X-ray structures mentioned above. This alleviates the computational cost associated with the QM−MM reaction path optimizations, which may present flaws when important conformational changes are involved.

Recently, it has been demonstrated that deoxyhemoglobin shows nitrite reductase activity, specially in tissue beds with low oxygen tension, indicating that the nitrite pool can induce systemic vasodilation and decreased blood pressure as an alternative source of NO.[38] The relevance of these results point at further experimental and theoretical studies of nitrite reductase activity of smooth muscle heme proteins, such as cytochrome P450, mitochondrial cytochromes, and, eventually, soluble guanylyl cyclase.

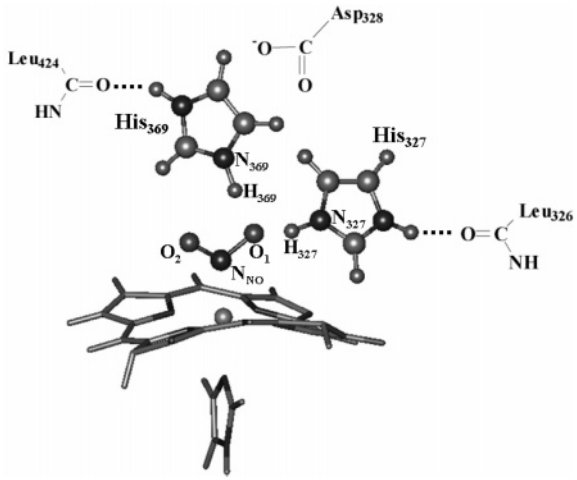

Figure 3. Relevant numbering of the QM subsystem of Pa NIR with nitrite bound (reactive). The neighboring residues, treated using MM and mentioned in the text are also shown schematically. The rest of the protein is omitted for clarity.

Model Systems and Computational Methods. We constructed initial structures for our calculations from the structure of the nitric oxide complex of the cd_1 NIR from *Pseudomonas aeruginosa* (PDB code 1NNO). Calculations were performed for a monomeric unit, from residue 26 to the end from chain α and from residue 1 to 25 from chain β. Histidine protonation was assigned favoring H bond formation. The system was solvated with TIP3P water molecules up to a distance of 30 Å of the d_1 heme center. A first step of a classical MM optimization was performed to relax the initial structure, followed by hybrid QM−MM geometry optimizations using a conjugate gradient algorithm. Only residues located less than 10 Å apart from the catalytic center were allowed to move freely. Calculations of the isolated QM system in a vacuum were also performed to assess the relevance of the protein environment effects.

All QM computations were performed at the DFT level with the SIESTA code.[39] The SIESTA method has shown an excellent performance for medium and large systems and has also proved to be appropriate for biomolecules, and specifically, for heme models.[40] The use of standard norm-conserving pseudopotentials[41] avoids the computation of core electrons, smoothing at the same time the valence charge density. In our study, the nonlinear partial-core correction[42] is applied to the iron atom. Basis functions consist of localized (numerical) pseudoatomic orbitals projected on a real space grid to compute the Hartree potential and exchange correlation potential matrix elements. For all atoms, basis sets of double ξ plus polarization quality were employed, with a pseudoatomic orbital energy shift of 25 meV and a grid cutoff of 150 Ry.[39] Calculations were performed using the generalized gradient approximation functional proposed by Perdew et al.[43] This combination of functional, basis sets, and grid parameters has been already validated for heme models.[40]

The classical subsystem was treated using the force field parameterization developed by Wang et al.[44]

We have selected the iron porphyrinate plus the ligands and the distal and proximal amino acids as the quantum subsystem (Figure 3). The rest of the protein unit mentioned above and the water molecules were treated classically. The final system consisted of 75 to 85 QM atoms and 11 466 MM atoms. The

TABLE 1: Histidine Proton Affinity and Nitrite Binding Energy[a,c]

proton affinity[b]	H_{369} (H_{327})	H_{327} (H_{369})	H_{327} (H_{369} H+)	H_{369} (H_{327} H+)
free enzyme:	−355.0	−333.7	−255.5	−274.6
nitrite bound:	−388.6	−374.6	−320.4	−333.0
nitrite binding:	H_{327} H_{369} +31.4	H_{369}+ H_{327} −4.1	H_{369} H_{327}+ −9.5	H_{327}+ H_{369}+ −67.8

[a] For comparison, the proton affinity of isolated imidazole in water is −294.0 kcal/mol. [b] Protonation state of the second histidine is shown in parentheses. [c] All energies are in kcal/mol.

frontier between the QM and MM portions of the system has been treated by the scaled position link atom method[45,46] adapted to our SIESTA code. Link atoms have been used in the proximal histidine and in the distal histidines 369 and 327 to separate the QM treated imidazol rings from the backbone of the amino acids. The ferrous unbound pentacoordinated heme group isolated or in the protein was treated as a high spin (HS) quintuplet state, which is known to be the ground state for this system.[26,27] The hexacoordinated bound ferrous or ferric heme groups were treated as low spin (LS) states; this state is known to be the ground state for this system.[26,27] More technical details about the QM−MM implementation can be found elsewhere.[47]

Ligand affinities(ΔE_L) were calculated as

$$\Delta E_L = E_{Enz-L} - E_L - E_{Enz}$$

where E_{Enz-L} is the energy of the ligand bound enzyme, E_{Enz-L} is the energy of the ligand free enzyme, and E_L is the energy of the isolated ligand in aqueous solution.

Obtaining accurate free energy profiles requires an extensive sampling, which is very difficult to achieve at the DFT QM−MM level. For this reason, we have computed the potential energy profiles using restrained energy minimizations along the reaction paths. For this purpose, an additional term is added to the potential energy according to $V(\xi) = k(\xi - \xi_0)^2$, where k is an adjustable force constant, ξ is the value of reaction coordinate in the system particular configuration, and ξ_0 is the reaction coordinate desired value. Varying ξ_0, the system is forced to follow the minimum reaction path along the given coordinate. This method has been successfully applied in QM−MM reaction path calculations.[47] Our choice for the reaction coordinate in the different steps will be shown later in the article.

Results and Discussion

Protonation State of the Histidines and Nitrite Binding. The first step for the nitrite reduction catalyzed by Pa NIR is nitrite binding to the d_1 heme active site. In the literature it is commonly accepted that both histidines are protonated in the substrate free enzyme.[7] To analyze in detail the relationship between the histidines' protonation state and nitrite binding affinity, we calculated the proton affinities of the histidines in the presence and absence of nitrite and the nitrite binding energy for the different protonation states. For comparison, the aqueous imidazol proton affinity was also calculated. (Table 1).

The nitrite binding energy to the ferrous pentacoordinated enzyme is probably large due to the high spin state of the heme group. Pure DFT functionals such as the one used in this work are known to overestimate the energy of high spin configurations,[26] and therefore it is expected that the binding energies should be also overestimated. However, the comparative analysis of the results for nitrite binding energies, reported in Table 1, still provides valuable information.[26]

The calculated proton affinity for both histidines was found to be similar (with a slight preference for His 369), suggesting that the first proton could go to any of both histidines. Visual analysis of the optimized structures showed that protonated His 369 was stabilized due to the hydrogen bonding between the proton bound to the Nϵ atom and the carbonyl oxygen of Leucine 424 (Figure 3). This hydrogen bond stabilizes extra charge density on the histidine ring to trap a second proton at the Nδ site. Moreover, the protonated His 369 was further stabilized by the carboxylate oxygen atoms of aspartic acid 328. On the other hand, the proton attached to Nϵ of His 327 exclusively formed one H bond with the carbonylic oxygen of residue Leucine 326. (Figure 3). The preference for the protonation of His 369 over His 327 in Pa NIR is consistent with the results obtained by Ranghino et al.,[31] who observed a preferential protonation of His 388 over His 345 in Pp NIR.

Once the first proton was bound, the affinity for the second one was found to be much lower. The proton affinity of the second histidine falls below the corresponding value for the aqueous imidazol proton affinity (with pK_a around 7). Therefore, it seems unlikely to find both histidines simultaneously protonated in the free enzyme. Subsequently, nitrite binding was only exergonic when at least one histidine was protonated, and it was more exergonic when the protonated one was His 327. Once the nitrite is bound, the affinity for the second proton became higher than that calculated for aqueous imidazol. It is interesting to remark that when both histidines were protonated the nitrite affinity increased dramatically as compared to the monoprotonated state. The results clearly show that there is a synergistic mechanism that favors the biprotonated nitrite bound state.

We also found that in all optimized structures the neutral histidines moved away (the Nδ shifts about 1.5 Å) from the active site and that the free Nδ atom formed hydrogen bonds with crystallographic waters. This flexibility may be relevant in proton trapping mechanisms from nearby water molecules.

Dehydration Reaction Pathway. To investigate the energy profile of the nitrite dehydration reaction, we proposed two possible scenarios. The first one is a concerted mechanism in which the oxygen atom of the nitrite reacts simultaneously with both protons of the histidines to form a water molecule, as depicted schematically in the path A of Figure 1. Second, we postulated two different two step mechanisms, in which a proton first migrates from one of the histidines to the coordinated nitrite. Then, the nitrous acid formed reacts with the second proton from the other histidine to yield a water molecule, as shown in the paths B and C of Figure 1. In all reaction energy profiles, the maximum of the potential energy along the reaction coordinate will be referred to as the apparent transition state (TS).

The QM−MM optimized structure of the reactant conformation is shown in Figure 3. For clarity, we show only the QM system and the MM residues in the vicinity of the active site. The relevant geometrical parameters for the nitrite and the resulting NO complex are shown in Table 2. It can be seen that the bound nitrite ion was already favorably oriented for the reaction, with the O_1 atom forming two hydrogen bonds with both H_{327} and H_{369}. It is interesting to notice that the H bond forming hydrogen atoms (H_{327} and H_{369}) remained at the same distance (about 1.5 Å) while the resulting $H_{369}-O_1-H_{327}$ angle was 105.0°, a value close to that of the water equilibrium angle. In the product, the H369−O_1−H327 angle of the resulting water was found to be 107.1°, a value very close to the initial value. An interesting fact about the product was that the calculated Fe−N_{NO}−O_2 angle (158.0°) and the net Mulliken charge found

TABLE 2: Relevant Structural Parameters (Å and Degrees) for the Nitrite Coordinated (Reactive) and Nitric Oxide Coordinated (Product) Enzyme Structures[a]

	reactant	product	free complex
NO charge (e)	-	0.21	0.26
$Fe-N_{NO}$	1.90	1.68	1.66
$N_{NO}-O_1$	1.39	2.54	-
$Fe-N_{NO}-O_2$	123.0	158.0	178.0
O_1-H_{369}	1.54	1.02	-
$H_{369}-N_{369}$	1.12	1.72	-
O_1-H_{327}	1.53	1.01	-
$H_{327}-N_{327}$	1.11	1.7	-
$H_{327}-O_1-H_{369}$	105.0	107.1	-

[a] Relevant parameters of the porphyrin Fe(III)-NO complex in a vacuum are also shown. (Labels of the atoms are given in Figure 3).

on the NO moiety (0.21 e) corresponded to a somewhat distorted $\{FeNO\}^6$ species, according to the Enemark and Felthan formalism.[48]

In this formalism, the linear NO group in the $\{FeNO\}^6$ species is assigned as NO^+ (isoelectronic with CO), and bent NO groups are assigned as NO or NO^- (isoelectronic with O_2).[42] Our results suggest that in the enzyme the $\{FeNO\}^6$ complex has more neutral NO character than in the isolated nitrosyl d_1 heme(III) complex, with an Fe−N−O angle of 178.0° and a Mulliken charge of 0.26 e (see Table 2). The results show that in the protein there are steric effects that distort the NO complex. This would lead to a weaker Fe−NO bond in the protein, due to a weaker π back donation (measured as the negative charge on the NO) and evidenced by a larger $Fe-N_{NO}$ distance compared to the isolated complex (Table 2). This suggests that the product is not in a completely optimal conformation for a $\{FeNO\}^6$ species and that this could possibly favor NO release.

The proposed concerted mechanism was analyzed using restrained energy minimizations along the selected reaction coordinate; the distance between the nitrogen and oxygen atoms of the nitrite ion $\xi = d(O_1-N_{NO})$ was used as the reaction coordinate (Figure 3), as mentioned above. The energetic reaction profile for the concerted mechanism is shown in Figure 4A. The computed barrier and the ΔE for the dehydration reaction were found to be 2.4 and −13.0 kcal/mol, respectively. The nitrite N−O distance was 1.39 Å in the reactant and 1.55 Å in the apparent transition state, indicating that the apparent transition state lies very close to the equilibrium geometry of the reactants.

For the two step mechanisms, we analyzed in the first place the proton transfer steps between each one of the histidines and the nitrite ion. The selected reaction coordinate was the position of the H to be transferred (H_{369} or H_{327}) relative to the donor and acceptor atoms $\xi = d(H-O_1)$. In the case of a proton migrating from His 327 yielding the intermediate shown schematically in path B of Figure 1, the energy barrier is only 1.6 kcal/mol and the whole reaction is slightly exergonic ($\Delta E = -0.8$ kcal/mol). In this case, the apparent transition state lies close to the intermediate where the proton is bound to the nitrite ion. In the resulting reaction intermediate, the N−OH distance in the formed nitrous acid is longer than in the starting nitrite ion (1.70 vs 1.39 Å). In the second step, stretching of this bond drives the reaction to products with a very shallow barrier (less than 0.1 kcal/mol), lying close to the reaction intermediate. The whole energetic profile is shown in Figure 4B.

When the proton is first placed on histidine 369 (path C of Figure 1), the calculated barrier is 1.7 kcal/mol and the proton transfer reaction is slightly endergonic (0.7 kcal/mol). The resulting intermediate also presents a longer N−OH distance than the starting structure (1.50 vs 1.39 Å). As in the other two

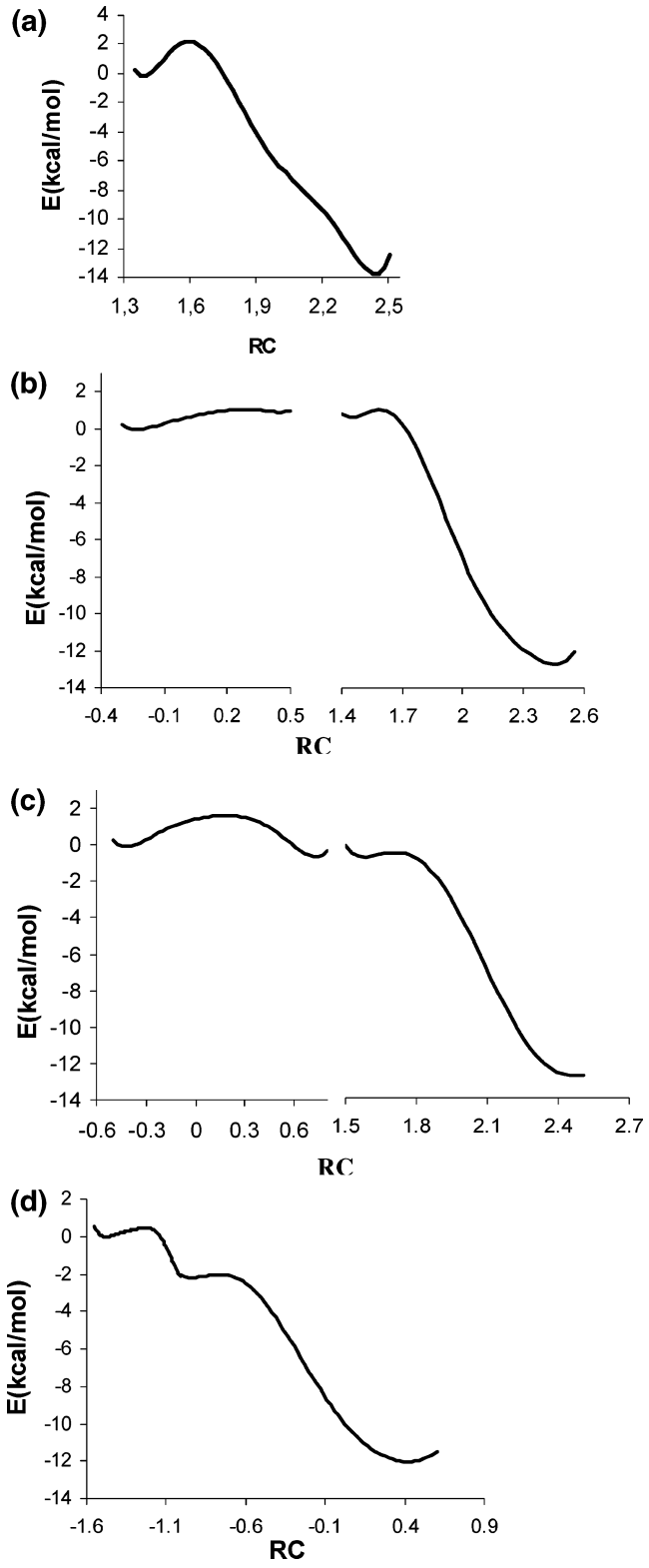

Figure 4. (A) Energy reaction profile for the concerted mechanism. The reaction coordinate is taken as the nitrite NO bond distance. (B) Energy reaction profile for the two step mechanism. The reaction coordinate is taken as the distance between the nitrite O and the transferred H in the first step and the nitrite NO distance in the second step. (C) Energy reaction profile for the two step mechanism. The reaction coordinate is taken as the distance between the nitrite O and the transferred H in the first step and the nitrite NO distance in the second step. (D) Energy reaction profile for the symmetric reaction coordinate.

step mechanism, the barrier for the second step is very low (0.6 kcal/mol) and the apparent transition state lies close to the

intermediate structure. The whole energetic profile is shown in Figure 4C. We have also performed a constrained optimization using a symmetric reaction coordinate, $\xi = d(O_1-N_{NO}) - [d(H_{327}-O_1) + d(H_{369}-O_1)]$. With this choice, the system can achieve the required proton transfer following the minimum energy path. The computed energy profile, shown in Figure 4D, shows that the process occurs by a two step mechanism. The first step consists of the transfer of H_{369}, with the second step consisting of the concerted O_1-N_{NO} bond breaking and $H_{327}-O_1$ bond formation.

Analyzing the proposed mechanisms, it is clear that both two step mechanisms are almost equivalent, as both have very similar barriers. The barrier for the concerted mechanism is higher. However, since barriers are low for all cases, both concerted and consecutive mechanisms could be operative at physiological conditions.

NO Release. A new cycle of nitrite reduction requires the release of NO and the reduction of the resultant d_1 heme Fe(III) by internal electron transfer from the *c* heme. X-ray, EPR,[49,50] and FTIR[51] experiments have confirmed the formation of the {FeNO}^{6} nitrosyl intermediate.[49,50] The subtle tuning of the stability of this intermediate is responsible for the regulation of NO release. The rate constants for NO displacement by water in isolated ferric porphyrinates is of the order of 103 s^{-1}.[52] On the other hand, the {FeNO}^{7} complex also detected is a very stable species unable to release NO, which drives the enzyme to a dead end, since the k_{off} in this case was estimated to be as low as 2×10^{-4} s^{-1}.[52] Additional evidence from Raman spectroscopy suggests that in this enzyme the Fe−NO bond in the {FeNO}^{7} species is particularly strong.[53]

The {FeNO}^{7}species probably arises from the back reaction of NO with the Fe(II) d_1 heme, or from reduction of the {FeNO}^{6} species.[51,54] As mentioned above, NO must be released and replaced by another ligand (probably water) before the reduction to an {FeNO}^{7} dead end species occurs. One possibility is that after NO escape the recently formed water molecule occupies the vacant distal space. The reaction is shown schematically in path B of Figure 2. To analyze this, we calculated the energetic change associated with the NO displacement by the recently formed water. The computed ΔE for this reaction is 42.7 kcal/mol. The reaction is highly endergonic, probably because the water molecule has to break two hydrogen bonds to displace the NO.

Another possibility is that another water molecule displaces the bound NO (Reaction shown schematically in path A of Figure 2). The estimated ΔE for NO displacement with another water molecule is about 17 kcal/mol. This value was calculated from the ΔE for the NO displacement reaction with an isolated water molecule in a vacuum (10.8 kcal/mol) and adding an estimated water desolvation energy (7 kcal/mol.). Although the reaction is endergonic, it is more feasible than the former one.

We also calculated the ΔE for the reaction of NO displacement by the crystallographic water molecule closest to the iron atom. We found a water molecule in the optimized structures at about 4.2 Å from the iron. Visual inspection of the QM−MM structures and X-ray data shows that there are several waters close to the active site. This is reasonable since the enzyme needs to exchange nitrite and water molecules with the environment to function properly. The ΔE for this reaction is 14.7 kcal/mol, which is a similar value to that obtained for the displacement with a bulk water molecule. The resulting optimized structures in both cases are almost equivalent.

Experimental activation enthalpies ($\Delta H\ddagger$) for NO release in ferric model porphyrins in water and for met-hemoglobin are 16.7 and 18.64 kcal/mol, respectively.[54] In both cases the reactions are quite fast ($k_{off} = 1 \times 10^3$ s^{-1} and 16 s^{-1}).[54] Our computed NO displacement energy, even though endergonic, is of similar magnitude of the above-mentioned experimental energies. Therefore, the hypothesis of NO displacement by a water molecule is consistent with the computed energy barrier of about 14 kcal/mol.

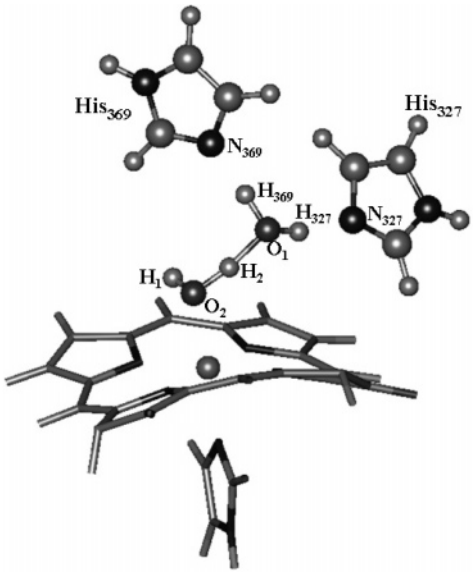

Figure 5. Relevant numbering of the QM subsystem of PA NIR showing the two water molecules complex.

TABLE 3: Relevant Structural Parameters (Å) for the Structure of the Enzyme with Two Water Molecules in the Active Site (Figure 5)

$Fe-O_2$	1.90
O_2-H_2	1.10
O_2-H_1	0.98
H_2-O_1	1.35
O_1-H_{369}	1.02
$H_{369}-N_{369}$	1.63
O_1-H_{327}	1.05
$H_{327}-N_{327}$	1.54

Our results also show that the enzyme presents an intermediate structure in which at least two water molecules are located in the active site. (Figure 5) Relevant structural parameters for the resulting complex with two water molecules in the active site are shown in Table 3.

This structure presents a possible mechanism for histidine reprotonation after one cycle of nitrite reduction. Binding of water to the iron(III) atom labilizes one proton, which can then easily migrate to the other water that is coordinated to the neutral histidines. The resulting hydronium cation (atoms H_2, O_1, H_{369}, and H_{327} in Figure 5) can transfer a proton to one of the histidines, resulting in a protonated histidine, a new water molecule, and an Fe(III)−OH configuration in the active site. We calculated the energy of the resulting configuration, which is only 1.7 kcal/mol higher than the energy of the configuration containing the two water molecules. The eventual escape of the new water molecule will lead to an active site with one protonated histidine and an iron coordinated by an hydroxide ion, a structure which has already been observed in X-ray structures of the oxidized state for Pa NIR. We also calculated the Fe(III)−OH active site configuration with either of the histidines protonated. The results under this situation show again that His 369 is more likely to be protonated (by 5.3 kcal/mol) than His 327.

TABLE 4: Electron Affinity and Conformational Relaxation Energy (kcal/mol) for the Different Complexes

	vertical electron affinity		conformational relaxation energy		adiabatic electron affinity	
complex	in a vacuum	in protein	in a vacuum	in protein	in a vacuum	in protein
Fe−NO	−122.4	−18.1	−20.0	−35.0	−142.4	−53.1
Fe−H_2O	−143.8	−28.0	−2.1	−19.7	−145.9	−47.7
Fe−NO_2^-	−60.3	−81.9	−2.5	−10.0	−70.3	−152.2

Reduction Step. It has been mentioned that to act efficiently the enzyme has to avoid reducing the d_1 heme before NO release to avoid getting trapped in the {FeNO}^{7} dead end species. To analyze the reduction energetics for different scenarios, we calculated the vertical electron affinity, the subsequent conformational relaxation, and the adiabatic or total electron affinity of the d_1 heme with different ligands and conformations for the isolated system in a vacuum treated fully at the QM level, and for the heme group in the enzyme treated using the QM−MM scheme. The same procedure was used to shed light on the electron transfer mechanisms in the photosynthetic reaction center.[56] Our computed results for both cases are shown in Table 4.

Clearly, electron transfer in the protein is more favorable when nitrite is bound. This is reasonable because Fe(II) stabilizes nitrite due to π back donation,[57] also making the oxygen atoms more negative and reinforcing the hydrogen bonds with the histidines. However, if electron transfer occurs once the nitrite is bound, it implies that nitrite originally bound to the oxidized enzyme, which has a poorer affinity for this ligand then the reduced enzyme.[7,57] However, the possibility cannot be completely ruled out.

Comparing the reduction energetics between the Fe−H_2O and Fe−NO complexes, the values for the vertical electron affinity slightly favor the reduction of the water complex. However, the conformational relaxation is larger in the nitrosyl complex, resulting in a larger adiabatic electron affinity. This reflects the fact that the conformations of the Fe(II) and Fe(III) nitrosyl complexes differ more than the corresponding water complexes, mainly because the transition from the {FENO}^{6} to {FENO}^{7} species involves the bending of the Fe−N−O angle (180 to 140° for isolated nitrosylporphyrins). Both in the protein and in a vacuum, the vertical electron affinity is larger in the aqueous complex, while the adiabatic electron affinity is slightly larger in the NO complex. This suggests that the enzyme does not make the reduction of the nitrosyl complex less favorable, but avoids ending in the Fe(II)−NO dead end species by displacing NO, and then reducing either the water complex, the free enzyme, or the nitrite complex that are stable in both oxidation states.

Conclusions

Reduction of nitrite to nitric oxide is the key step in bacterial denitrification, a process with enormous environmental implications. Besides the reduction step, it is essential to understand the specific role of the protein environment on the NO product release from the heme center. This mechanism is relevant for getting a deeper understanding of the regulation of other important heme proteins such as soluble guanylate cyclase and nitric oxide synthase, among others.

The aim of this work was to analyze in detail the complete nitrite reduction cycle in Pa NIR by using a DFT based QM−MM scheme that allows us to study the active site immersed in the whole protein environment. Our study provides a more realistic picture of NIR reactivity than former QM studies performed using stripped down models of the active site.[31]

Our results for Pa NIR agree with those obtained using a model system for Pp NIR[31] in the following aspects:

(i) The histidine stabilized by a nearby aspartic acid (His 369 in Pa and His 388 in Pp) is more likely to be protonated than the other.

(ii) Nitrite binding affinity is greatly enhanced when both histidines are protonated.

(iii) The resulting {FeNO}^{6} complex can be better described as an Fe(III)−NO complex with the NO in a bent conformation. It has been suggested that the orientation of nitric oxide could arise as a consequence of the nonequivalence of the iron surrounding nitrogen atoms of the d_1 heme or because of distal interactions.[31] Our results with the isolated nitrosyl complex in the d_1 heme in a vacuum (Table 2) yielding a linear NO as expected for Fe(III)−NO complexes rule out the first possibility and support the idea that NO orientation is controlled mainly by distal interactions.

On the other hand, there are differences regarding the NO escape mechanism between the two species. In Pp NIR, Ranghino et al.[31] showed that NO escape is probably assisted by Tyr 25 that can bind to the iron in the oxidized state. In our work with Pa NIR, Tyr 10 is too far away to bind to the iron, and our results show that NO is probably displaced by a water molecule different from the one formed in the dehydration process. (path A of Figure 2).

The detailed and complete mechanism for the Pa NIR reaction, predicted from our QM−MM calculations, can be summarized as follows:

(i) The resting reduced state of the enzyme is probably monoprotonated in histidine 327.

(ii) Nitrite binding is thermodynamically favorable in the mono- or biprotonated active site.

(iii) Once nitrite is bound, it increases the proton affinity of the second histidine by more than 60 kcal/mol. The fact that the unprotonated Nδ of the histidine forms several hydrogen bonds with nearby water molecules gives support to a substrate bound biprotonated active site.

(iv) The dehydration reaction occurs with a very low barrier (less than 2.4 kcal/mol) either in a concerted or a two step mechanism, resulting in an {FeNO}^{6} complex and a water molecule hydrogen bonded to the histidines. Taking into account that nitrite binds to the monoprotonated active site, it is also possible that, instead of a nitrite ion, a nitrous acid molecule binds to the enzyme or that once nitrite is bound the second proton goes to the nitrite ion proton instead of going to the histidine, leading directly to the reaction intermediate of one of the two step mechanisms.

(v) The resulting {FeNO}^{6} complex exhibits NO in an sterically nonoptimal conformation for such a complex (as can be seen from the QM−MM optimized Fe−N−O angle and the NO Mulliken charge). This will facilitate NO displacement, probably by a water molecule avoiding reduction to the dead end Fe(II)−NO complex. The resulting structure has two water molecules in the active site and can reorder the protons to leave an Fe(III)−OH^- complex and a protonated histidine.

(vi) Internal electron transfer reduces the Fe(III) metal center, leaving a water molecule or a hydroxide ion coordinated to the

Fe(II). Fe(II) has poor affinity for water or OH^-, so the ligand is easily lost, leaving the free enzyme ready for a new cycle.

The results presented here show that the catalytic capacity of the enzyme lies primary in the position and environment of the distal histidines that can act as proton donors and acceptors in the enzyme's active site. Our results suggest that NO displacement is the limiting step of the whole reaction, since the involved proton transfers exhibit low barriers. Experimental confirmation of this hypothesis may be obtained by performing kinetic isotope effects studies. The flexibility of the active site cavity and solvent accessibility play an important role as well. Our results also shed light on the structural requirements for nitrite reduction catalyzed by other heme proteins, a process that has recently been proposed to play a key role in the NO physiological regulation in anoxic tissues.[38]

Acknowledgment. We acknowledge J. A. Olabe for bringing this subject to our attention and A. Roitberg for carefully reading the manuscript and useful discussions. This work was partially supported by the University of Buenos Aires, Agencia Nacional de Promoción Científica y Tecnológica (ANPCYT, Argentina), CONICET, and Fundación Antorchas.

References and Notes

(1) Zumft, W. G. *Microbiol. Mol. Biol. Rev.* **1997**, *61*, 5333−616.
(2) Yamanake, T.; Ota, A.; Okunuki, K. *Biochim. Biophys. Acta* **1961**, *53*, 294−308.
(3) Greenwod, C.; Barber, D.; Parr, S. R.; Antonini, E.; Brunori, M.; Colosimo, A. *Biochem. J.* **1978**, *173*, 11−17.
(4) Horio, T.; Higashi, T.; Sasagawa, M.; Kusai, K.; Nakai, M.; Okunki, K. *Biochem. J.* **1960**, *77*, 194−201.
(5) Averill, B. A.; Tiedje, M. *FEBS Lett.* **1982**, *138*, 8.
(6) Enemark, J. H.; Feltham, R. D. *Coord. Chem. Rev.* **1974**, *13*, 339.
(7) Wasser, I. M.; de Vries, S.; Moenne Loccoz, P.; Schroeder, I.; Karlin. K. D. *Chem. Rev.* **2002**, *102*, 1201−1234.
(8) Yamanaka, T. S.; Kijinoto, S.; Okumuki, K. *J. Biochem*. **1963**, *53*, 416−421.
(9) Rainey, F. A. *Int. J. Syst. Bacteriol.* **1999**, *49*, 645−651.
(10) Moir, J. W. B.; Baratta, D.; Richardson, D. J.; Ferguson, S. J. *Eur. J. Biochem*. **1993**, *212*, 377−385.
(11) Timkovich, R.; Dhesi, R.; Martinkus, K. J.; Robinson, M. K.; Rea. T. M. *Arch. Biochem. Biophys*. **1982**, *215*, 47−58.
(12) Weeg-Ardessen, E.; Wu, W.; Ye, R. W.; Tledje, J. M.; Chang, C. K. *J. Biol. Chem.* **1991**, *266*, 7496−7502.
(13) Nurizzo, D.; Silvestrini, M. C.; Mathieu, M.; Cutruzzola, F.; Bourgeois, D.; Fulop, V.; Hajdu, J.; Brunori, M.; Tegoni, M.; Cambillau, C. *Structure* **1997**, *5*, 1157.
(14) Nurizzo, D.; Cutruzzola, F.; Arese, M.; Bourgeois, D.; Brunori, M.; Cambillau, C.; Tegoni, M. *Biochemistry* **1998**, *37*, 13987.
(15) Chang, C. K.; Barkigia, K. M.; Hanson, L. K.; Fajer, J. *J. Am. Chem. Soc.* **1986**, *108*, 1352.
(16) Cutruzzola, F.; Brown, K.; Wilson, E. K.; Bellelli, A.; Arese, M.; Tegoni, M.; Cambillau, C.; Brunori, M. *Proc. Nat. Acad. Sci. U.S.A.* **2001**, *98*, 2232−2237.
(17) Silvestrini, M. V.; Galeotti, C. L.; Gervais, M.; Schinina, E.; Barra, D.; Bossa, F.; Brunori, M. *FEBS Lett.* **1989**, *254*, 3367.
(18) Cheesman, M. R.; Ferguson, S. J.; Moir, J. W. B.; Richardson, D. J.; Zumpft, W. G.; Thompson, A. *Biochemistry* **1997**, *36*, 16267.
(19) Allen, J. W. A.; Watmough, N. J.; Ferguson, S. J. *Nat. Struct. Biol.* **2000**, *7*, 885.
(20) Loew, G. H.; Harris, D. L. *Chem. Rev.* **2000**, *100*, 407−419.
(21) Siegbahn, P. E. M.; Blomberg, M. R. A. *Chem. Rev.* **2000**, *100*, 421.
(22) Sigfridsson, E.; Ryde, U. *J. Biol. Inorg. Chem.* **1999**, *4*, 99.
(23) Schoneboom, J. C.; Lin, H.; Reuter, N.; Thiel, W.; Cohen, S.; Ogliaro, F.; Shaik, S. *J. Am. Chem. Soc.* **2002**, *124* (27), 8142−8151.
(24) Scherlis, D. A.; Cymeryng, C. B.; Estrin, D. A. *Inorg. Chem.* **2000**, *39* (11), 2352−2359.
(25) Rovira, C.; Kunc, K.; Hutter, J.; Ballone, P.; Parrinello, M. *J. Phys. Chem. A* **1997**, *101*, 8914.
(26) Scherlis, D. A.; Martí, M. A.; Ordejón, P.; Estrin, D. A. *Int. J. Quantum Chem.* **2002**, *90* 1505−1514.
(27) Scherlis, D. A.; Estrin, D. A. *J. Am. Chem. Soc.* **2001**, *123*, 8436.
(28) Tsukamoto, K.; Nakamura, S.; Shimizu, K. *J. Mol. Struct. THEOCHEM* **2003**, *624*, 309−322.
(29) Einsle, O.; Messerschmidt, A.; Huber, R.; Kroneck, P. M. H.; Neese, F. *J. Am. Chem. Soc.* **2002**, *124*, 11737−11745.
(30) Ghosh, A.; Wondimagegn, T. *J. Am. Chem. Soc.* **2000**, *122*, 8101.
(31) Ranghino, G.; Scorza, E.; Sjorgen, T.; Williams, P. A.; Ricci, M.; Hajdu, J. *Biochemistry* **2000**, *39*, 10958−10966.
(32) Warshel, A.; Levitt, M. *J. Mol. Biol.* **1976**, *103*, 227.
(33) Zhang, X.; Harrison, D. H. T.; Cui, Q. *J. Am. Chem. Soc.* **2002**, *124* (50), 14871−14878.
(34) Faulder, P. F.; Tresadern, G.; Chohan, K. K.; Scrutton, N. S.; Sutcliffe, M. J.; Hillier, I. H.; Burton, N. A. *J. Am. Chem. Soc.* **2001**, *123* (35), 8604−8605.
(35) Ridder, L.; Harvey, J. N.; Rietjens, I. M. C. M.; Vervoort, J.; Mulholland, A. J. *J. Phys. Chem. B.* **2003**, *107* (9), 2118−2126.
(36) Diaz, N.; Suarez, D.; Sordo, T. L.; Merz, K. M., Jr. *J. Am. Chem. Soc.* **2001**, *123* (31), 7574−7583.
(37) Devi-Kesavan, L. S.; Gao, J. *J. Am. Chem. Soc*. **2003**, *125* (6), 1532−1540.
(38) Cosby, K.; Partovi, K. S.; Crawford, J. H.; Patel, R. P.; Reiter, C. D.; Martyr, S.; Yang, B. K.; Waclawiw, M. A.; Zalos, G.; Xu, X.; Huang, K. T.; Shields, H.; Kim-Shapiro, D. B.; Schechter, A. N.; O'Cannon, R.; Gladwin, M. T. *Nature Medicine* **2003**, *9*, 1498−1505.
(39) Soler, J. M.; Artacho, E.; Gale, J.; García, A.; Junquera, J.; Ordejón, P.; Sánchez-Portal, D. *J. Phys: Condens. Matter* **2002**, *14*, 2745.
(40) Martí, M. A.; Scherlis, D. A.; Doctorovich, F. A.; Ordejón, P.; Estrin, D. A. *J. Biol. Inorg. Chem.* **2003**, *6*, 595−600.
(41) Troullier, N.; Martins, J. L. *Phys. Rev. B* **1991**, *43*, 1993.
(42) Louie, S. G.; Froyen, S.; Cohen, M. L. *Phys. Rev. B* **1982**, *26*, 1738.
(43) Perdew, J. P.; Burke, K.; Ernzerhof, M. *Phys. Rev. Lett.* **1996**, *77*, 3865.
(44) Wang, J.; Cieplak, P.; Kollman, P. A. *J. Comput. Chem.* **2000**, *21*, 1049.
(45) Eichinger, M.; Tavan, P. *J. Chem. Phys.* **1999**, *110* (21), 10452.
(46) Rovira, C.; Schultze, B.; Eichinger, M.; Evanseck, J. D.; Parrinello, M. *Biophys J.* **2001**, *81*, 435.
(47) Crespo, A.; Scherlis, D. A.; Martí, M. A.; Ordejón, P.; Roitberg, A. E.; Estrin, D. A. *J. Phys. Chem. B* **2003**, *107*, 13728−13736.
(48) Richter-Addo, G. B.; Legzdins, P. *Metal Nitrosyls*; Oxford University Press: New York, 1992.
(49) Williams, P. A.; Fulop, V.; Garman, E. F.; Saunders, N. F. W.; Ferguson, S. J.; Hadju, J. *Nature* **1997**, *389*, 406.
(50) Silvestrini, M. C.; Tordi, M. G.; Musci, G.; Brunori, M. *J. Biol. Chem.* **1990**, *265*, 11783.
(51) Wang, Y.; Averill, B. A. *J. Am. Chem. Soc.* **1996**, *118*, 3972.
(52) Laverman, L. E.; Ford, P. C. *J. Am. Chem. Soc.* **2001**, *123*, 11614−11622.
(53) Kanti Das, T.; Wilson, E. K.; Cutruzzola, F.; Brunori, M.; Rousseau, D. L. *Biochemistry* **2001**, *40*, 10774−10781.
(54) George, S. J.; Allen, J. W. A.; Ferguson, S. J.; Throneley, R. N. F. *J. Biol. Chem.* **2000**, *275*, 33231.
(55) Wanat, A.; Gdula-Argasinska, J.; Rutkowska-Zbik, D.; Witko, M.; Stoechel, G.; Van Eldick, R. *J. Biol. Inorg. Chem.* **2002**, *7*, 165−176.
(56) Hasegawa, J.; Ishida, M.; Nakatsuji, L. Z.; Liu, H.; Yang W. *J. Phys. Chem. B* **2003**, *107*, 838−847.
(57) Finnegan, M. G.; Lappin, A. G.; Scheidt, R. W. *Inorg. Chem.* **1990**, *29*, 181−185.